

Phase separation in antisymmetric films: A molecular dynamics study

Raishma Krishnan,¹ Prabhat K. Jaiswal,² and Sanjay Puri¹

¹*School of Physical Sciences, Jawaharlal Nehru University, New Delhi 110067, India*

²*Institut für Physik, Johannes Gutenberg-Universität Mainz, Staudinger Weg 7, D-55099 Mainz, Germany*

(Received 23 August 2013; accepted 17 October 2013; published online 5 November 2013)

We have used molecular dynamics (MD) simulations to study phase-separation kinetics in a binary fluid mixture (AB) confined in an antisymmetric thin film. One surface of the film (located at $z = 0$) attracts the A-atoms, and the other surface (located at $z = D$) attracts the B-atoms. We study the kinetic processes which lead to the formation of equilibrium morphologies subsequent to a deep quench below the miscibility gap. In the initial stages, one observes the formation of a layered structure, consisting of an A-rich layer followed by a B-rich layer at $z = 0$; and an analogous structure at $z = D$. This multi-layered morphology is time-dependent and propagates into the bulk, though it may break up into a laterally inhomogeneous structure at a later stage. We characterize the evolution morphologies via laterally averaged order parameter profiles; the growth laws for wetting-layer kinetics and layer-wise length scales; and the scaling properties of layer-wise correlation functions. © 2013 AIP Publishing LLC. [<http://dx.doi.org/10.1063/1.4827882>]

I. INTRODUCTION

In recent years, there has been much research activity, both theoretical and experimental, on the behavior of fluid mixtures in confined geometries, e.g., pores, slits, and films.^{1–4} The effect of wetting surfaces on domain growth has been one of the major research problems in this area.^{3,4} In this paper, we study the phase-separation kinetics of a binary mixture (AB) confined in a thin film with *antisymmetric* boundaries. The lower surface of the film attracts one species (say, A) and the upper surface attracts the other species (B). This gives rise to an enrichment of the preferred components at the surfaces. The effect of such antisymmetric walls has been studied earlier in the context of phase-separation dynamics in Ising systems,^{5,6} polymer blends,⁷ and binary mixtures.^{8,9}

To understand the relevant equilibrium morphologies, consider an immiscible AB mixture, placed in contact with a surface (S) having a preferential attraction for A. The system shows either a *completely wet* (CW) or a *partially wet* (PW) equilibrium morphology, depending upon the relative surface tensions between A, B, and S.^{10,11} In the CW morphology, the AB interface is parallel to the surface. In the PW morphology, the interface between the A-rich and B-rich domains meets the surface at a contact angle θ determined by *Young's condition*¹⁰

$$\gamma_{AB} \cos \theta = \gamma_{BS} - \gamma_{AS}. \quad (1)$$

Here, γ_{AB} is the surface tension between the A-rich and B-rich phases; and γ_{AS}, γ_{BS} are the surface tensions between the A-rich and B-rich phases and S. In thin films of thickness D , finite-size effects significantly affect the above transitions. What are the counterparts of the PW and CW morphologies discussed above for $D \rightarrow \infty$? For an antisymmetric film, the PW morphology consists of a trapezoidal plug with appropriate contact angles at the lower and upper surfaces – see

Fig. 1(a). On the other hand, the CW morphology consists of domains of A-rich and B-rich phases with an interface parallel to the film surfaces – see Fig. 1(b).

In the present work, we are interested in the kinetic processes which lead to the formation of these equilibrium morphologies subsequent to a deep quench from the high-temperature disordered state to the low-temperature segregated state. In the absence of confinement, the evolution is usually referred to as *spinodal decomposition* (SD).^{12–14} During SD, there is an emergence of A-rich and B-rich domains, characterized by a single time-dependent length scale $L(t)$. The kinetics of phase separation in bulk systems has received much attention, and we will quote relevant results shortly.

We use molecular dynamics (MD) simulations to study the kinetics of binary fluids at surfaces. The homogeneous AB mixture at high temperatures is confined between two surfaces located at $z = 0, D$ along the z -direction. The system is quenched deep below the miscibility curve at time $t = 0$, due to which it segregates into A-rich and B-rich domains. Further, the bottom surface of the system gets wetted by A particles, and the top surface gets wetted by B particles. The interplay between these two dynamical processes, namely, wetting and phase separation, is referred to as *surface-directed spinodal decomposition* (SDSD) or *surface-directed phase separation*. There exist many experimental^{3,15–17} and theoretical works^{4,8,9,18–21} on this problem. However, to the best of our knowledge, there has been no study of SDSD for fluid mixtures in antisymmetric films. This area of research has many important technological applications, including the fabrication of nanoscale patterns and multi-layered structures.²²

This paper is organized as follows. In Sec. II, we describe our model and provide details of the MD simulations. In Sec. III, we present detailed numerical results. Finally, Sec. IV concludes this paper with a summary and discussion.

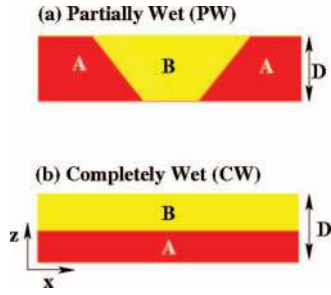


FIG. 1. Schematic of equilibrium morphologies for an antisymmetric thin film of size $L \times L \times D$: the lower surface (at $z = 0$) attracts A and the upper surface attracts B. The A-rich domains are marked red, and the B-rich domains are marked yellow. A phase transition between the (a) *partially wet* (PW) and (b) *completely wet* (CW) morphologies arises in the limit $D \rightarrow \infty$.

II. MODEL

We consider an AB fluid mixture of point particles confined in a box of volume $V/\sigma^3 = L \times L \times D$, where σ is the Lennard-Jones (LJ) particle diameter. Periodic boundary conditions are applied in the x - and y -directions. We introduce impenetrable surfaces or walls at $z = 0$ and $z = D$.^{9,23} These walls give rise to an integrated LJ potential ($\alpha = A, B$)

$$u_w(z) = \frac{2\pi n\sigma^3}{3} \left[\frac{2\epsilon_r}{15} \left(\frac{\sigma}{z'} \right)^9 - \delta_\alpha \epsilon_a \left(\frac{\sigma}{z'} \right)^3 \right], \quad (2)$$

where $n = N/(L^2D) = 1$ is the fluid density. In Eq. (2), ϵ_r and ϵ_a are the strengths of the repulsive and attractive parts of the surface potential: ϵ_r keeps the particles within the region, and ϵ_a determines the number of particles at the surfaces. For the bottom surface (at $z = 0$), we set $\delta_A = 1$ and $\delta_B = 0$, so that this surface attracts the A particles and repels the B particles. Further, $z' = z + \sigma/2$ so that the singularity of $u_w(z)$ occurs at $z = -\sigma/2$, which is outside the box. A similar surface is present at the top ($z = D$) with $z' = D + \sigma/2 - z$, and with $\delta_A = 0$ and $\delta_B = 1$. The top surface attracts B particles and repels A particles.

The particles within the system interact via the LJ potential

$$u(r_{ij}) = 4\epsilon_{\alpha\beta} \left[\left(\frac{\sigma}{r_{ij}} \right)^{12} - \left(\frac{\sigma}{r_{ij}} \right)^6 \right], \quad (3)$$

where $r_{ij} = |\vec{r}_i - \vec{r}_j|$. We set the interaction parameters as $\epsilon_{AA} = \epsilon_{BB} = 2\epsilon_{AB} = \epsilon$. The bulk phase diagram for this potential is well-known.²⁴ We use the truncated LJ potential with the cutoff $r_c = 2.5\sigma$ – this potential is shifted and force-corrected.²⁵ Further, we consider a high-density (incompressible) fluid with a critical composition: $N_A = N_B = N/2$. The particles have equal masses ($m_A = m_B = m = 1$); and we set $\sigma = 1$, $\epsilon = 1$, $k_B = 1$ so that the MD time unit is

$$t_0 = \sqrt{\frac{m\sigma^2}{48\epsilon}} = \frac{1}{\sqrt{48}}. \quad (4)$$

The MD runs were performed using the *velocity Verlet algorithm*²⁶ with a time-step $\Delta t = 0.07$ in MD units. We maintain the temperature (T) constant via the Nosé-Hoover thermostat which is known to preserve hydrodynamics.^{26,27}

The homogeneous initial state for a run was prepared by equilibrating the system at high T with periodic boundary conditions in all directions. At time $t = 0$, the system is quenched to $T = 1$, which lies below $T_c \simeq 1.423$. Further, the wetting surfaces are introduced at $z = 0$ and $z = D$. All statistical data presented in this paper are obtained as an average over 50 independent runs.

As mentioned earlier, we study the far-from-equilibrium dynamics of the quenched system. Subsequently, we will show the evolution snapshots which arise during surface-directed phase separation. We characterize the morphology by studying the layer-wise correlation functions and the length scales.¹⁸ The layer-wise correlation function is defined as

$$C_{\parallel}(\vec{\rho}, z, t) = L^{-2} \int d\vec{\sigma} [\langle \psi(\vec{\sigma}, z, t) \psi(\vec{\sigma} + \vec{\rho}, z, t) \rangle - \langle \psi(\vec{\sigma}, z, t) \rangle \langle \psi(\vec{\sigma} + \vec{\rho}, z, t) \rangle], \quad (5)$$

where the angular brackets denote statistical averaging over different runs.

In Eq. (5), we denote the coordinates parallel to the surface as $\vec{\rho}$. The order parameter $\psi(\vec{\rho}, z, t)$ is defined in terms of the local densities $n_\alpha(\vec{r}, t)$ as

$$\psi(\vec{\rho}, z, t) = \frac{n_A - n_B}{n_A + n_B}. \quad (6)$$

We define the order-parameter field at the centres of boxes of size $(2\sigma)^2 \times (1\sigma)$. Since the system is translationally invariant and isotropic in the (xy) -plane, C_{\parallel} does not depend on the direction of $\vec{\rho}$. We define the z -dependent lateral length scale $L_{\parallel}(z, t) \equiv L(z, t)$ from the decay of $C_{\parallel}(\rho, z, t)$

$$C_{\parallel}(\rho = L, z, t) = 0.1 \times C_{\parallel}(0, z, t). \quad (7)$$

For convenience, we denote $C_{\parallel}(\rho, z, t)$ as $C(\rho, t)$ in the following discussion. In bulk systems, the correlation function exhibits *dynamical scaling*^{12–14}

$$C(\vec{r}, t) = g\left(\frac{r}{L}\right), \quad (8)$$

where $g(x)$ is independent of time. This property indicates that the evolution morphology is statistically self-similar in time, and only the scale of the morphology changes. In our thin-film problem, dynamical scaling arises subsequent to the formation of well-formed laterally segregated domains.

To obtain the correlation function, a coarse-graining procedure²⁸ is employed, which is the numerical counterpart of the *renormalization group* (RG) technique. We divide our system into small boxes of size $(2\sigma)^2 \times (1\sigma)$, and count the total number of A and B particles in each box and its nearest neighbors. If there are more particles of A than B, we assign a “spin” value $S = +1$ located at the centre of the box. On the other hand, the box is given a spin value $S = -1$ when there are more B particles than A. Furthermore, when equal numbers of A and B particles are present, we assign $S = +1$ or -1 randomly. The correlation function is computed for this “hardened” order-parameter field $S(\vec{r}, t)$ from the definition in Eq. (5). By this coarse-graining method, it is possible to eliminate the fluctuations while preserving the important morphological features.

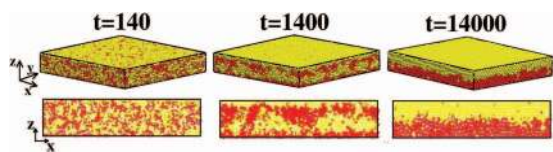


FIG. 2. Evolution snapshots (upper frames) for SDS in a binary Lennard-Jones (LJ) mixture confined in an antisymmetric thin film of size $L \times L \times D$ with $L = 64$ and $D = 10$. We show pictures at three different times: $t = 140$, $t = 1400$, and $t = 14000$. An impermeable wall located at $z = 0$ attracts A particles (marked red), and another impermeable wall at $z = D$ attracts B particles (marked yellow). The surface field strengths are $\epsilon_r = 0.5$ and $\epsilon_a = 0.6$. The temperature is $T = 1.0 \simeq 0.7T_c$. The lower frames represent the xz -cross-sections of the upper frames at $y = 0$.

We also computed the laterally averaged order parameter profiles [$\psi_{av}(z, t)$ vs. z]; and the wetting-layer thickness $R_1(t)$. The laterally averaged order parameter is obtained by averaging $\psi(\vec{\rho}, z, t)$ in the directions parallel to the surfaces, namely, the x - and y -directions. This is then further averaged over 50 independent runs. The wetting-layer thickness is defined as the first zero-crossing of $\psi_{av}(z, t)$.

Before we present our MD results, it is relevant to briefly discuss alternative approaches using continuum Langevin models. The appropriate coarse-grained model for phase-separating fluids is known as *Model H*,²⁹ and consists of coupled Langevin equations for the order parameter and fluid velocity fields.^{12,13} The velocity field obeys the *incompressibility condition* and it is not straightforward to implement this in the presence of a surface which breaks translational invariance. Tanaka and Araki^{30,31} have presented results from a simulation of Model H in a semi-infinite system, i.e., with one surface. To the best of our knowledge, there are no results available for Model H in a thin-film geometry with either symmetric or antisymmetric surfaces. It would be useful to compare our microscopic MD results with those from a continuum Ginzburg-Landau (GL) simulation. However, it is not simple to obtain a direct mapping between MD and GL time-scales.

III. DETAILED NUMERICAL RESULTS

In this section, we present detailed results from our MD simulations of SDS in antisymmetric films. In Fig. 2, we show the evolution snapshots and their corresponding yz -cross-sections for a film with thickness $D = 10$. We show pictures at three different times: $t = 140$, $t = 1400$, and $t = 14000$. The surface field strengths considered are $\epsilon_r = 0.5$ and $\epsilon_a = 0.6$, which correspond to a CW morphology in equilibrium. An A-rich layer (marked red) develops at the surface $z = 0$, and a B-rich layer (marked yellow) develops at the surface $z = D$. The snapshots and their cross-sections demonstrate that, at intermediate times, the surface develops a layered morphology with a wetting layer of A followed by a depletion layer of A at $z = 0$. At $z = D$, there is an analogous wetting layer of B followed by its depletion layer. At late times ($t = 14000$), the system evolves into the equilibrium CW state with A at the bottom surface and B at the top surface.

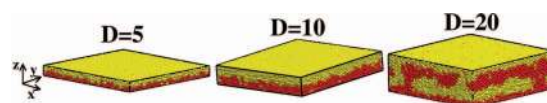


FIG. 3. Evolution snapshots at $t = 14000$ for three different system sizes with $L = 64$ and $D = 5$, $D = 10$ and $D = 20$. The other details are the same as in Fig. 2.

Figure 3 shows a comparison of the evolution snapshots at $t = 14000$ for three different film thicknesses: $D = 5$, $D = 10$, and $D = 20$. We can see that the system has reached its equilibrium state for $D = 5$ and $D = 10$. However, for $D = 20$, the system is still evolving towards its final state. As expected, thicker films take longer to reach the equilibrium state due to trapping in intermediate metastable states.

Many experimental probes which use depth-profiling techniques do not have any lateral resolution, and yield only laterally averaged order parameter profiles.³ As mentioned earlier, these are obtained from our simulations by averaging the order parameter along the x - and y -directions, and then taking an ensemble average. In Fig. 4, we plot the average depth profiles [$\psi_{av}(z, t)$ vs. z] for $D = 5$, $D = 10$, and $D = 20$. The order parameter is positive (A-rich) at $z = 0$ and negative (B-rich) at $z = D$, as the film surfaces attract different components. The profiles at early times ($t = 140$) show the presence of two SDS waves, originating from the top and bottom surfaces and propagating towards the center of the film.¹⁵ At the film center, $\psi_{av}(z, t) \simeq 0$, due to the antisymmetry of the film. This is similar to the symmetric film studied by Das *et al.*,⁹ where there are also two SDS waves. However, unlike the

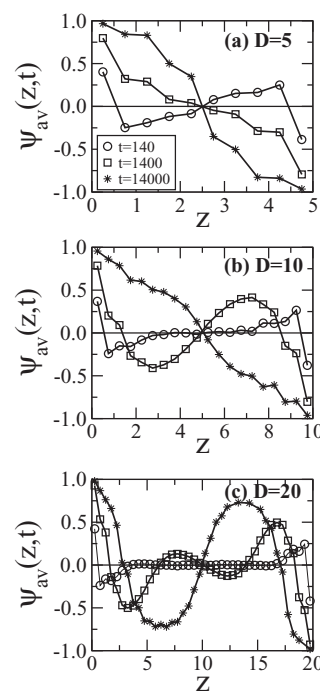


FIG. 4. Laterally averaged order parameter profiles for an antisymmetric film at times $t = 140$, $t = 1400$, and $t = 14000$ for (a) $D = 5$, (b) $D = 10$, and (c) $D = 20$. These are obtained from the evolution snapshots as described in the text. The symbols denote the same times in (a), (b), and (c). The surface field strengths are $\epsilon_r = 0.5$ and $\epsilon_a = 0.6$.

present study, both the SDSD waves are in anti-phase when they interfere as both the surfaces attract the same species. The interactions of such SDSD waves may give rise to complex morphologies, e.g., in mixtures that are in contact with physically and chemically patterned substrates.³² These systems have important technological applications in controlling the transport of fluid mixtures in micro-channels.

In Fig. 4(a) (for $D = 5$), the two SDSD waves interact for all times considered. In Fig. 4(b) (for $D = 10$), the order parameter profile for $t = 140$ starts from $\psi_{av} \simeq +0.5$ at $z = 0$ and then decays to bulk-like behavior ($\psi_{av} \simeq 0$) in the middle of the film. The two SDSD waves interact at intermediate times ($t = 1400$) and coalesce at later times ($t = 14000$) to form the equilibrium CW morphology. For the film with thickness $D = 20$ [see Fig. 4(c)], there is no coalescence of the waves even for $t = 14000$ (see Fig. 3, $D = 20$ frame). Thus, one can see the formation of the CW state at $t = 14000$ for both $D = 5$ and $D = 10$. However, for $D = 20$, the equilibrium state is accessed much later. For even thicker films, the system becomes permanently trapped in metastable multi-layered states.

The evolution profiles in Fig. 4 are characterized by $R_1(t)$, which is the first zero-crossing of $\psi_{av}(z, t)$. This quantity measures the wetting-layer thickness. In Fig. 5, we show data for $R_1(t)$ vs. t for the three different system sizes considered, namely, $D = 5$, $D = 10$, and $D = 20$. The system reaches equilibrium with $R_1 \simeq D/2$ at $t \simeq 700$ for $D = 5$, and $t \simeq 5000$ for $D = 10$. However, the system is still evolving towards its final state for $D = 20$, as we have already seen in Figs. 3 and 4.

In Fig. 6, we present a comparison of $R_1(t)$ vs. t for $D = 5$, 10, 20 with two different surface field strengths: $\epsilon_a = 0.2$ and $\epsilon_a = 0.6$. In both cases, the equilibrium morphology is CW. We see that weaker fields drive the system faster to equilibrium, which is somewhat counter-intuitive. For $\epsilon_a = 0.2$, the system with $D = 20$ has also equilibrated by $t = 14000$. This is because stronger fields give rise to a multi-layered structure at early times, which propagates into the bulk more slowly; and is destabilized on much longer time-scales.

In Fig. 7, we present cross-sections from the MD evolution for $D = 20$. The frames on the left show the xy -cross-sections (parallel to the surfaces) of the SDSD snapshot in

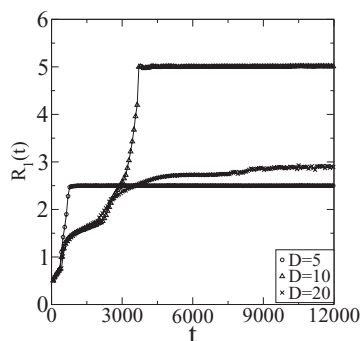


FIG. 5. Time-dependence of the first zero-crossing $R_1(t)$ of the laterally averaged profiles, which gives a measure of the wetting-layer thickness. We show data for three different system sizes: $D = 5$, $D = 10$, and $D = 20$. The system reaches the equilibrium CW state at $t \simeq 700$ for the $D = 5$ case, and $t \simeq 4000$ for the $D = 10$ case.

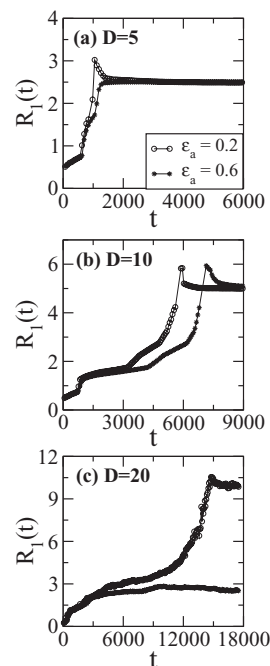


FIG. 6. Time-dependence of $R_1(t)$ for film thicknesses (a) $D = 5$, (b) $D = 10$, and (c) $D = 20$ with two different ϵ_a -values, namely, $\epsilon_a = 0.2$ and $\epsilon_a = 0.6$.

Fig. 3 for $D = 20$ at $t = 14000$. We show cross-sections for three layers: the top frame corresponds to $z \in (0, 1)$ (the bottom layer), the middle frame corresponds to $z \in (4, 5)$, and the bottom frame corresponds to $z \in (9, 10)$ (middle layer). These slices are labeled as $z = 0.5$, $z = 4.5$, and $z = 9.5$, respectively. The frames on the right show the corresponding coarse-grained pictures of the S -field obtained as described in Sec. II. We can see that the bottom layer of the film has almost no B atoms, and appears all red due to the elimination of fluctuations by the coarse-graining procedure. As stated earlier, we use these coarse-grained pictures to compute the correlation functions.

Next, we study the layer-wise correlation functions and length scales. In Fig. 8, the left-hand frames are scaling plots

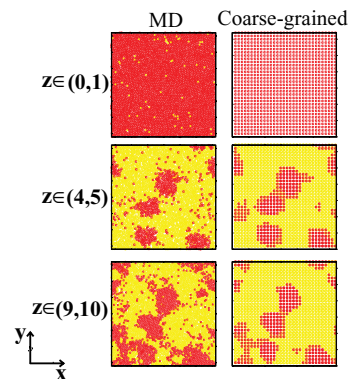


FIG. 7. Cross-sections of SDSD snapshots (frames on the left). We show slices in the xy -plane for system size $D = 20$ at $t = 14000$. The frames on the right show the coarse-grained versions of the MD snapshots. The A-atoms are marked red, and the B-atoms are marked yellow. The top frame corresponds to $z \in (0, 1)$ or the bottom layer; the middle frame corresponds to $z \in (4, 5)$; and the bottom frame corresponds to $z \in (9, 10)$ or the middle layer.

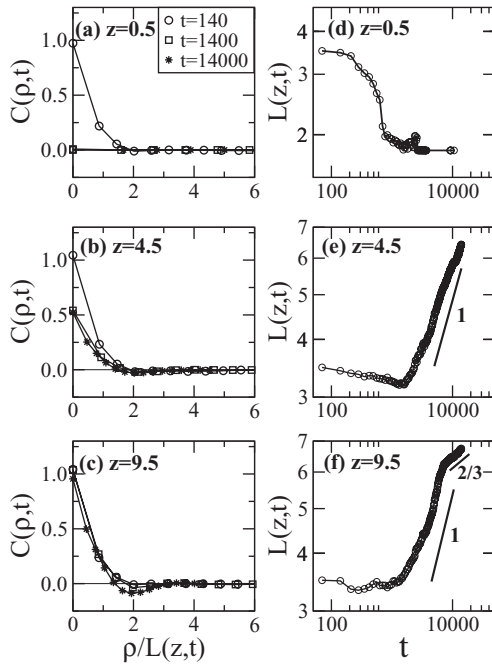


FIG. 8. Left-hand frames show plots of the layer-wise correlation function, $C(\rho, t)$ vs. $\rho/L(z, t)$, at $t = 140, t = 1400$, and $t = 14000$. The film thickness is $D = 20$. We show data for (a) $z = 0.5$, (b) $z = 4.5$, (c) $z = 9.5$. The right-hand frames show the time-dependence of the layer-wise length scale, $L(z, t)$ vs. t , for (d) $z = 0.5$, (e) $z = 4.5$, (f) $z = 9.5$. The length-scale data are plotted on a log-log scale.

of $C(\rho, t)$ vs. $\rho/L(z, t)$ for $D = 20$. The layer-wise length-scale $L(z, t)$ is defined in Eq. (7). Figure 8(a) corresponds to $z = 0.5$ (bottom layer). At the earliest time ($t = 140$), there are both A and B particles in this layer [see the laterally averaged profile at $t = 140$ in Fig. 4(c)]. The corresponding correlation function in Fig. 8(a) decays smoothly from its maximum value: $C(\rho, t) = 1$ at $\rho = 0$. At later times, the bottom layer consists primarily of A-atoms. For a configuration with all A-atoms, the definition in Eq. (5) yields $C(\rho, t) = 0$. This explains the flat correlation functions at $t = 1400, 14000$ in Fig. 8(a). Figure 8(b) corresponds to $z = 4.5$. In Fig. 4(c), we see that $\psi_{av}(z = 4.5, t)$ evolves from $\psi_{av} \simeq 0$ at $t = 140$ to $\psi_{av} \simeq -0.7$ at $t = 14000$. It is known that the scaled correlation function for bulk phase separation depends explicitly on the degree of off-criticality.³³ Hence, the plot in Fig. 8(b) does not show dynamical scaling in the time-window considered. Finally, Fig. 8(c) corresponds to $z = 9.5$ (film center). At the center, $\psi_{av} \simeq 0$ for all t [see Fig. 4(c)], in spite of the complex pattern dynamics in the rest of the film. This is a consequence of the antisymmetric nature of the film. Thus, we expect dynamical scaling to be recovered at $z = 9.5$, which is confirmed by Fig. 8(c).

In Figs. 8(d)–8(f), we show the time-dependence [$L(z, t)$ vs. t] of the layer-wise length scales at $z = 0.5, 4.5, 9.5$. These data are plotted on a log-log scale. Figure 8(d) corresponds to $z = 0.5$, where the length scale is only meaningful in the early stages. The value of $L(z, t)$ saturates when the surface is completely coated by A-atoms with a corresponding flat correlation function [$C(\rho, t) = 0$]. In Figs. 8(e) and 8(f), we see a systematic growth of the length scale over the simulation time-window. The growth law is approximately linear (L

$\sim t$) at $z = 4.5$ in Fig. 8(e). The bulk phase-separation kinetics of 3- d fluids exhibits three growth regimes: $L(t) \sim t^\phi$ with the growth exponent ϕ showing a cross-over from $1/3$ (diffusive regime) to 1 (viscous hydrodynamic regime) to $2/3$ (inertial hydrodynamic regime).^{12–14} To date, MD simulations have only been able to evolve up to the $\phi = 1$ regime^{23,27} – the same is true for the data in Fig. 8(e). The length-scale data in Fig. 8(f) (for $z = 9.5$, film center) shows signs of a crossover from $L \sim t^1$ to $L \sim t^{2/3}$ at $t_c \sim 10000$. Notice that the crossover from the initial no-growth regime to t^1 -growth is somewhat later in Fig. 8(e) ($t_0 \sim 1600$) than in Fig. 8(f) ($t_0 \sim 1100$). This is because the layer $z \simeq 4.5$ has slightly off-critical composition due to the inward propagation of the SDSD wave – see Fig. 4(c). This off-criticality tends to suppress hydrodynamic effects due to the reduction of domain connectivity.

We associate the $t^{2/3}$ -regime in Fig. 8(f) with segregation in 2- d fluid mixtures rather than the inertial regime of 3- d fluids. The Brownian-dynamics simulations of Farrell and Valls³⁴ have shown that domain growth in 2- d fluids is characterized by $\phi \simeq 2/3$. In our case, the system becomes effectively two-dimensional due to the formation of the layered state. A similar $t^{2/3}$ -regime has also been observed during SDSD of fluid mixtures in symmetric films by Das *et al.*⁹

IV. SUMMARY AND DISCUSSION

Let us conclude this paper with a summary and discussion of our results. We have presented results from MD studies of SDSD in an antisymmetric thin film. We considered a binary (AB) fluid mixture with critical composition: $N_A = N_B = N/2$. The lower and upper surfaces of the film attracted A and B, respectively, with equal field strengths. The temperature was maintained below the critical temperature ($T < T_c$) by a Nosé-Hoover thermostat, which is known to preserve hydrodynamic interactions. Therefore, our study naturally incorporates fluid velocity fields, and generalizes previous studies of diffusion-driven SDSD in an antisymmetric film.⁸

The wetting surfaces give rise to opposite SDSD waves, which propagate towards the center of the film. We consider surface fields which give rise to a CW equilibrium morphology, as depicted in Fig. 1(b). For thin films, the propagating SDSD waves coalesce smoothly and form this CW state. However, for thicker films, the system can evolve into intermediate metastable states with very long life-times. Such states also arise for stronger surface fields which give rise to a multi-layered morphology. These metastable states are of great experimental significance, and our numerical simulations suggest experimental methods to stabilize nonequilibrium (transient) structures in confined geometries.

We have also studied the length scales associated with the SDSD morphologies, viz., the wetting-layer thickness $R_1(t)$; and the layer-wise length scale $L(z, t)$. The wetting-layer thickness settles to its equilibrium value ($R_1 = D/2$) after a transient regime, which may be very extended as discussed above. On the other hand, $L(z, t)$ shows growth kinetics consistent with bulk phase separation in fluid mixtures,^{12,13} especially at the center of the film where $\psi_{av} \simeq 0$.

The subject of phase separation in confined geometries continues to be interesting and still presents many open issues. We hope that the theoretical results presented here will provoke further experimental and theoretical interest in these problems.

ACKNOWLEDGMENTS

R.K. gratefully acknowledges DST for financial support through a DST Fast-track project [SR/FTP/PS-12/2009].

- ¹R. Evans, *J. Phys. Condens. Matter* **2**, 8989 (1990); A. O. Parry, *ibid.* **8**, 10761 (1996).
- ²L. D. Gelb, K. E. Gubbins, R. Radhakrishnan, and M. Sliwinski-Bartkowiak, *Rep. Prog. Phys.* **62**, 1573 (1999).
- ³G. Krausch, *Mater. Sci. Eng. R.* **R14**, 1 (1995); M. Geoghegan and G. Krausch, *Prog. Polym. Sci.* **28**, 261 (2003).
- ⁴S. Puri, and H. L. Frisch, *J. Phys. Condens. Matter* **9**, 2109 (1997); S. Puri, *ibid.* **17**, R101 (2005); K. Binder, S. Puri, S. K. Das, and J. Horbach, *J. Stat. Phys.* **138**, 51 (2010).
- ⁵K. Binder, D. Landau, and M. Muller, *J. Stat. Phys.* **110**, 1411 (2003).
- ⁶E. V. Albano, K. Binder, and W. Paul, *J. Phys. Condens. Matter* **12**, 2701 (2000).
- ⁷M. Muller and K. Binder, *Phys. Rev. E* **63**, 021602 (2001).
- ⁸S. K. Das, S. Puri, J. Horbach, and K. Binder, *Phys. Rev. E* **72**, 061603 (2005).
- ⁹S. K. Das, S. Puri, J. Horbach, and K. Binder, *Phys. Rev. E* **73**, 031604 (2006); *Phys. Rev. Lett.* **96**, 016107 (2006).
- ¹⁰T. Young, *Philos. Trans. R. Soc. London* **95**, 65 (1805).
- ¹¹J. W. Cahn, *J. Chem. Phys.* **66**, 3667 (1977); M. E. Fisher, *J. Stat. Phys.* **34**, 667 (1984); P. G. de Gennes, *Rev. Mod. Phys.* **57**, 827 (1985); S. Dietrich, in *Phase Transitions and Critical Phenomena*, edited by C. Domb and J. L. Lebowitz (Academic Press, London, 1988), Vol. 12, p. 1.
- ¹²*Kinetics of Phase Transitions*, edited by S. Puri and V. K. Wadhawan (CRC Press, Boca Raton, FL, 2009).
- ¹³A. J. Bray, *Adv. Phys.* **43**, 357 (1994); K. Binder, and P. Fratzl, in *Phase Transformations in Materials*, edited by G. Kostorz, (Wiley, Weinheim, 2001), p. 409.
- ¹⁴A. Onuki, *Phase Transition Dynamics* (Cambridge University Press, Cambridge, 2002).
- ¹⁵R. A. L. Jones, L. J. Norton, E. J. Kramer, F. S. Bates, and P. Wiltzius, *Phys. Rev. Lett.* **66**, 1326 (1991).
- ¹⁶G. Krausch, C.-A. Dai, E. J. Kramer, and F. S. Bates, *Phys. Rev. Lett.* **71**, 3669 (1993).
- ¹⁷J. Liu, X. Wu, W. N. Lennard, and D. Landheer, *Phys. Rev. B* **80**, 041403 (2009); C.-H. Wang, P. Chen, and C.-Y. D. Lu, *Phys. Rev. E* **81**, 061501 (2010).
- ¹⁸S. Puri and K. Binder, *Phys. Rev. A* **46**, R4487 (1992); *Phys. Rev. E* **49**, 5359 (1994); *J. Stat. Phys.* **77**, 145 (1994); S. Puri, K. Binder, and H. L. Frisch, *Phys. Rev. E* **56**, 6991 (1997).
- ¹⁹G. Brown and A. Chakrabarti, *Phys. Rev. A* **46**, 4829 (1992); J. F. Marko, *Phys. Rev. E* **48**, 2861 (1993).
- ²⁰S. Puri and K. Binder, *Phys. Rev. Lett.* **86**, 1797 (2001); *Phys. Rev. E* **66**, 061602 (2002).
- ²¹L.-T. Yan and X. M. Xie, *J. Chem. Phys.* **128**, 034901 (2008); L.-T. Yan, J. Li, and X. M. Xie, *ibid.* **128**, 224906 (2008).
- ²²*Multilayer Thin Films: Sequential Assembly of Nanocomposite Materials*, edited by G. Decker and J. B. Schlenoff (Wiley-VCH, Weinheim, 2002).
- ²³P. K. Jaiswal, S. Puri, and S. K. Das, *J. Chem. Phys.* **133**, 154901 (2010); *Europhys. Lett.* **97**, 16005 (2012); *Phys. Rev. E* **85**, 051137 (2012).
- ²⁴S. K. Das, J. Horbach, and K. Binder, *J. Chem. Phys.* **119**, 1547 (2003).
- ²⁵M. P. Allen and D. J. Tildesley, *Computer Simulation of Liquids* (Clarendon Press, Oxford, 1987).
- ²⁶*Monte Carlo and Molecular Dynamics of Condensed Matter Systems*, edited by K. Binder and G. Ciccotti (Italian Physical Society, Bologna, 1996).
- ²⁷S. Ahmad, S. K. Das, and S. Puri, *Phys. Rev. E* **82**, 040107 (2010); **85**, 031140 (2012).
- ²⁸S. K. Das and S. Puri, *Phys. Rev. E* **65**, 026141 (2002).
- ²⁹P. C. Hohenberg and B. I. Halperin, *Rev. Mod. Phys.* **49**, 435 (1977).
- ³⁰H. Tanaka and T. Araki, *Europhys. Lett.* **51**, 154 (2000).
- ³¹H. Tanaka, *J. Phys. Condens. Matter* **13**, 4637 (2001).
- ³²P. Das, P. K. Jaiswal, and S. Puri, (unpublished).
- ³³Y. Oono and S. Puri, *Phys. Rev. Lett.* **58**, 836 (1987); *Phys. Rev. A* **38**, 434 (1988); S. Puri and Y. Oono, *ibid.* **38**, 1542 (1988).
- ³⁴J. E. Farrell and O. T. Valls, *Phys. Rev. B* **40**, 7027 (1989); **42**, 2353 (1990).

The Journal of Chemical Physics is copyrighted by the American Institute of Physics (AIP). Redistribution of journal material is subject to the AIP online journal license and/or AIP copyright. For more information, see <http://ojps.aip.org/jcpo/jcpcr/jsp>